Supporting Information for

A Molecular Dual-Center Emitter for Ratiometric Optical Thermometry

Rong Sun,[a †] Hong Huang,[b †] Ye Xia,[b] Youchao Liu,[b] Xingquan Tao,[b] Jun-Long Zhang,[a] Bing-Wu Wang[a,c*], and Song Gao[a,d*]

[a] Beijing National Laboratory for Molecular Sciences, College of Chemistry and Molecular Engineering, Peking University; Beijing, 100871, *P. R. China*. E-mail: wangbw@pku.edu.cn; gaosong@pku.edu.cn

[b] Spin-X Institute, School of Chemistry and Chemical Engineering, South China University of Technology, Guangzhou 510641, *P. R. China*.

[c] School of Chemical Engineering, Guizhou Minzu University, Guiyang 550025, *P. R. China*.

[d] Guangdong Basic Research Center of Excellence for Functional Molecular Engineering, School of Chemistry, Sun Yat-sen University; Guangzhou, 510275, *P. R. China*.

† These authors contributed equally to this work.

1. Experimental Procedures

Synthesis.

All experiments were conducted under aerobic conditions using analytically pure solvents. Lanthanide nitrate salts and (1R,2R)-(+)-1,2-diphenylethylenediamine were purchased from Energy Chemical. The phenolic ligand [6,6'-((1E,1'E)-(((1R,2R)-1,2-diphenylethane-1,2-diyl)bis(azaneylylide-ne))bis(methaneylylidene))bis(2-methox-yphenol)] (1*R*,2*R*-H_2L) was synthesized following a literature procedure[S1]. **ZnSm** crystals were grown via solvothermal method by dissolving 1*R*,2*R*-H_2L (0.06 mmol, 0.0327 g), $Zn(OAc)_2 \cdot 2H_2O$ (0.06 mmol, 0.0196 g), and $Sm(NO_3)_3 \cdot {}_5H_2O$ (0.03 mmol, 0.0177 g) in 5 mL methanol. The solution was heated at 75 °C overnight in a sealed Schlenk tube, resulting in the formation of large colorless single crystals of 1*R*,2*R*-ZnLSm(OAc)$(NO_3)_2$ on the inner wall. Elemental analysis (%) calcd. for $C_{32}H_{29}SmN_4O_{12}Zn$: C, 43.7; H, 3.3; N, 6.3. Found: C, 43.64; H, 3.1; N, 6.21.

For the preparation of **ZnGd**, a mixture of H_2L (0.06 mmol, 0.0327 g), $Zn(OAc)_2 \cdot 2H_2O$ (0.06 mmol, 0.0196 g), and $Gd(NO_3)_3 \cdot 5H_2O$ (0.03 mmol, 0.0177 g) in methanol (5 mL) was heated at 70 °C for 4 hours in a sealed Schlenk tube, yielding a white precipitate. The precipitate was collected by filtration, washed with dichloromethane, and dried. The product was then dissolved in dichloromethane and crystallized via ether diffusion. After one-week diffusion, transparent block-shaped crystals were obtained. Elemental analysis (%) calcd. for $C_{32}H_{29}GdN_4O_{12}Zn$: C, 43.5; H, 3.3; N, 6.3. Found: C, 43.58; H, 3.1; N, 6.24.

Preparation of **ZnSm@PMMA** film: First, **ZnSm** (2 mg) and polymethyl methacrylate (PMMA) (1200 mg) were dispersed in 3 ml toluene. The mixture was stirred at 70 °C for 1 hour to form homogeneous solution. This solution was then drop-cast onto a pre-cleaned glass substrate. A free-standing film was subsequently obtained by heating the substrate until the film spontaneously detached.

Single-Crystal Structure Determination.

Single crystals suitable for X-ray diffraction (XRD) were selected under an optical microscope. Diffraction data were collected using graphite-monochromatized Mo Kα radiation (λ = 0.71073 Å) at 150(2) K on an Agilent Bruker D8 diffractometer. Data collection, cell refinement, and reduction were performed using the CrysAlisPro software package.[S2] The structure was solved by direct methods using SHELXS and SHELXL[S3] Final refinements included anisotropic displacement parameters for all non-hydrogen atoms. The structure was checked for missed symmetry using the ADDSYM algorithm in PLATON,[S4] and no higher symmetry was detected. Crystallographic parameters, data collection, and refinement details are summarized in Table S1.

Elemental Analysis.

Elemental analyses for C, H, and N were performed on an EA1110 microelemental analyzer to confirm the phase purity of the complexes.

Thermal Stability.

Thermogravimetric analysis (TGA) was performed on a TGA-550 instrument by heating the sample from room temperature to 800 °C under a nitrogen atmosphere at a heating rate of 10 °C min^{-1}. Differential scanning calorimetry (DSC) measurements were conducted on a Netzsch DSC 204 F1 thermal analyzer under flowing nitrogen, with a heating rate of 10 °C min^{-1} from room temperature to 400 °C.

UV-Vis Measurements.

UV-Vis absorption spectra were recorded on a JASCO V-780 UV-Vis-NIR spectrophotometer over the wavelength range of 200–800 nm.

Powder XRD Analysis.

Powder X-ray diffraction (PXRD) measurements for the **ZnSm** sample were carried out on a Rigaku Miniflex 600 diffractometer equipped with a Cu Kα radiation source (λ = 1.5418 Å) and an incident-beam monochromator. Data were collected over a 2θ range of 5–50° with a step size of 0.02° and a fixed counting time of 0.20 s per step.

Emission Spectrum.

Emission and excitation spectra of the samples were recorded using a Horiba FluoroMax fluorescence spectrometer. Temperature-dependent emission spectra of the toluene solutions of **ZnSm** and **ZnGd** were measured on the same instrument equipped with an Oxford OPTISTAT-CFS temperature control system. Luminescence decay curves were obtained on an Edinburgh Instruments F920 spectrometer under excitation at 365 nm.

2. Theoretical Calculations

For the calculation of the energy levels of the ZnL moiety, the Sm(III) ion was replaced by the closed-shell rare-earth ions La(III), Y(III), and Lu(III), yielding **ZnLa**, **ZnY**, and **ZnLu**, respectively. Geometry optimizations and electronic-structure calculations were then carried out using density functional theory (DFT) as implemented in Gaussian 16[S5]. The CAM-B3LYP functional [S6] with long-range correction was employed, and solvent effects were included. The Stuttgart-Dresden relativistic effective core potential (SDD)[S7, S8] basis set was used for La(III)/Y(III)/Lu(III), the 6-31G(d,p)[S9] basis set for Zn, and the 6-31G(d) [S10] basis set for all remaining atoms. The DFT results for **ZnLa**, **ZnY**, and **ZnLu** were very similar (Table S4), and only the energy levels of **ZnLa** are discussed in the main text.

For the calculation of the energy levels of the Sm(III) ion, *ab initio* calculations were performed using the OpenMOLCAS[S11] package. The computational fragments were constructed directly from the crystallographic structures without further geometry optimization. Basis sets for all atoms were taken from the ANO-RCC library[S12, S13]: ANO-RCC-VTZP for Sm, VTZ for the nearest O atoms, and VDZ for more distant atoms. The second-order Douglas–Kroll–Hess Hamiltonian was employed, with scalar relativistic effects included in the contracted basis sets. Spin-orbit coupling was treated within the restricted active space state interaction (RASSI-SO)[S14, S15] approach. The active space comprised all seven 4f orbitals of Sm(III) with five active electrons (CAS(5,7)) in the CASSCF calculations, and dynamic correlation energies were further accounted for using the CASPT2[S16] module. Calculations were carried out both with and without inclusion of solvent effects, and the results were found to be very similar (Table S5 and S6). In the gas-phase calculation (without solvent effects), we mixed the maximum number of spin-free states that could be handled by our hardware (all 21 sextets, 128 out of 224 quadruplets, and 130 out of 490 doublets for the Sm(III) fragment). When solvent effects were included, an energy cutoff of 40,000 cm^{-1} was applied, and only spin-free states below this threshold were mixed (all 21 sextets, 108 quadruplets, and 60 doublets for the Sm(III) fragment). The results including solvent effects are shown in Figure 2c.

3. Supporting Figures

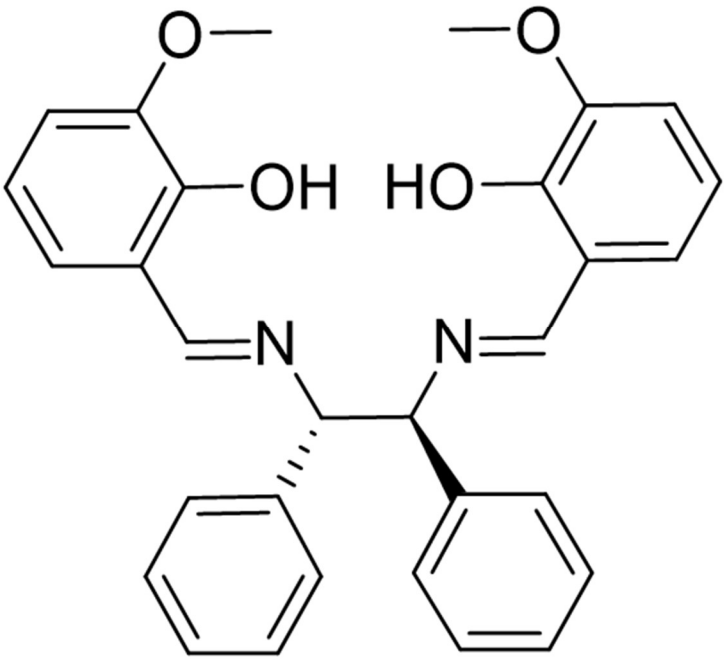

Scheme S1. Structure of the enantiopure **1*R*, 2*R*-H_2L**.

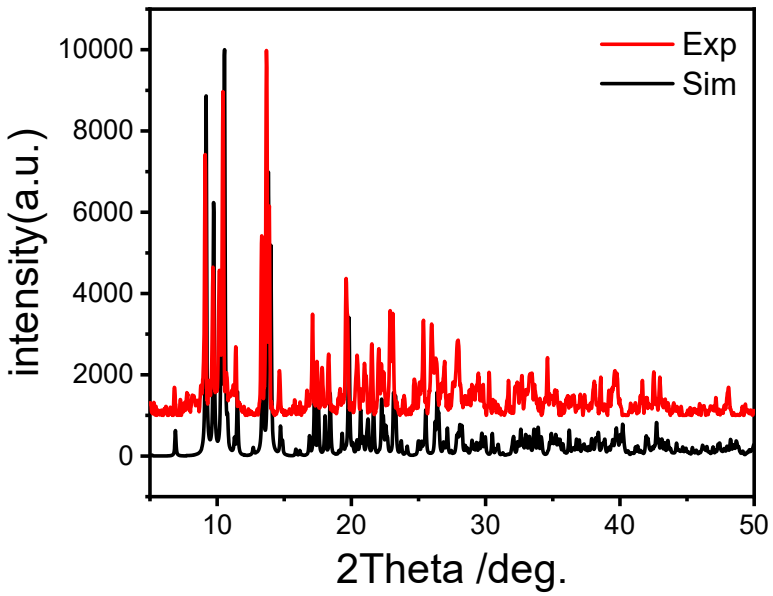

Figure S1. Experimental and simulated XRD patterns of **ZnSm**.

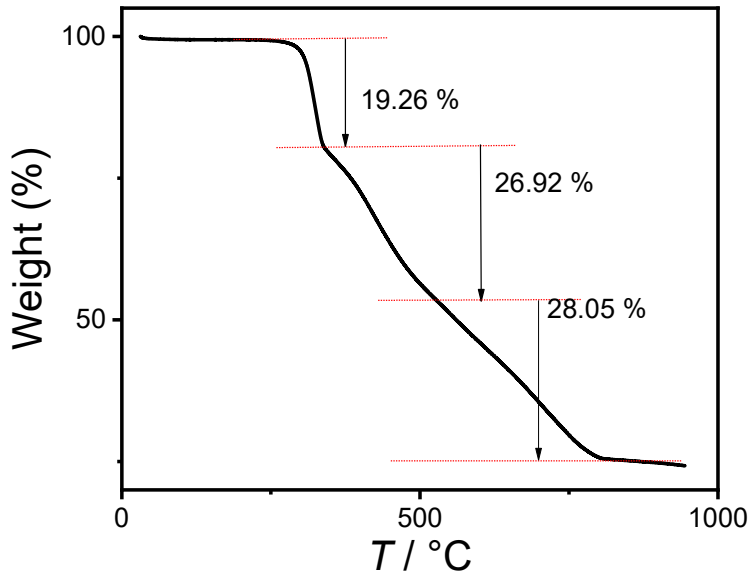

Figure S2. TGA curves of **ZnSm** (temperature in °C). Under a nitrogen atmosphere, the initial weight loss of 19.26% is attributed to the decomposition of the acetate group and the redox reaction between the nitrate groups and metal ions (calcd 20.86%). The subsequent two weight-loss steps correspond to the decomposition of the ligand, with the accelerated rate observed in the second stage arising from the breakdown of the imine groups within the ligand. The final residues are metallic Zn and Sm formed through reactions with the nitrate groups (found 25.38%, calcd 24.59%).

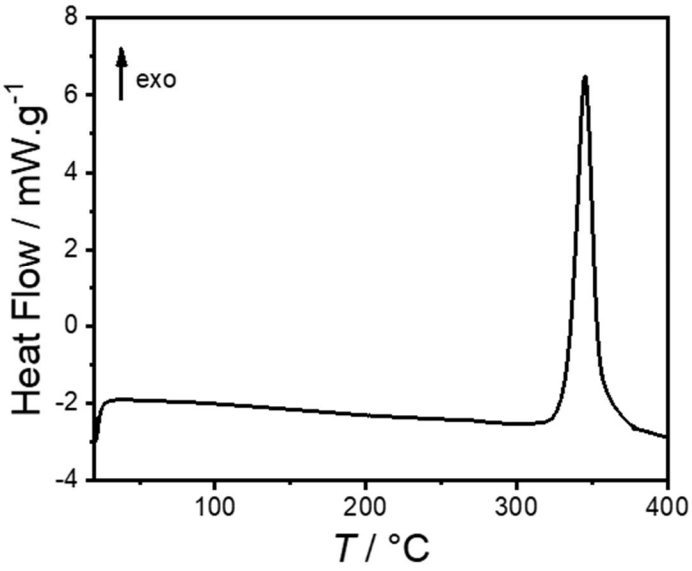

Figure S3. DSC curve of **ZnSm** recorded under a nitrogen atmosphere. The peak at approximately 340 °C is attributed to the thermal decomposition of the complex.

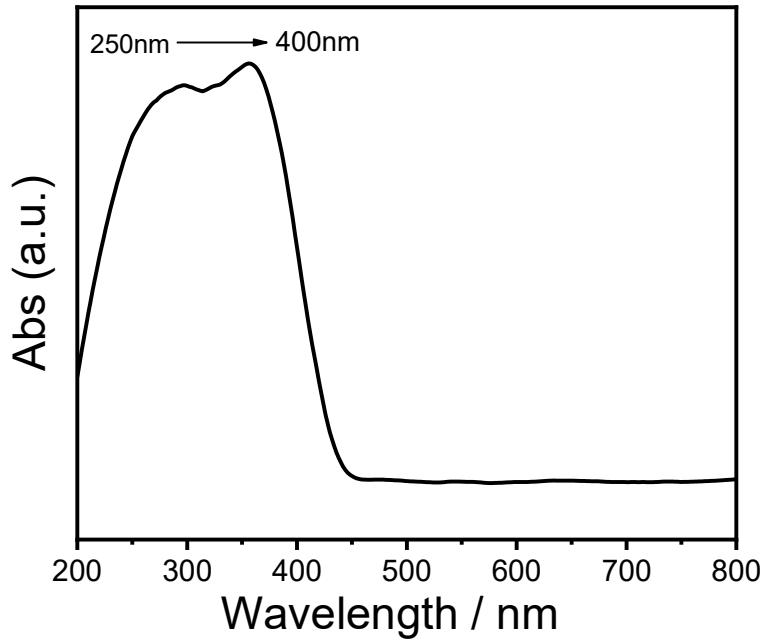

Figure S4. Solid-state UV-Vis spectrum of **ZnSm**. The complex exhibits a broad absorption band between 250 and 400 nm, which is mainly attributed to ligand-centered π-π* transitions and ligand-to-metal charge transfer (LMCT) transitions involving the imine nitrogen atoms and the Zn^{2+} center. Coordination to Zn^{2+} increases the degree of electron delocalization within the ligand framework, leading to a broadened absorption band and a slight red shift due to a reduced HOMO-LUMO energy gap.

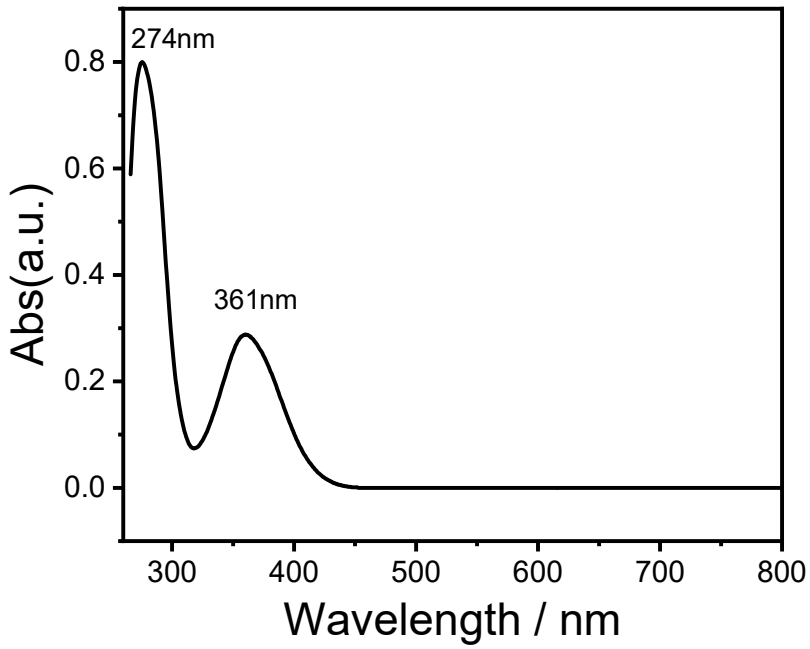

Figure S5. UV-Vis spectrum of **ZnSm** in toluene. **ZnSm** exhibits two distinct absorption bands at 274 and 361 nm, which are assigned to the π-π* transitions of the aromatic rings and the imine group, respectively. Compared with the broad absorption observed in the solid state, the spectrum in solution appears significantly narrower, likely due to the more homogeneous molecular environment in solution and the reduction of intermolecular interactions, which diminishes electronic coupling between neighboring molecules.

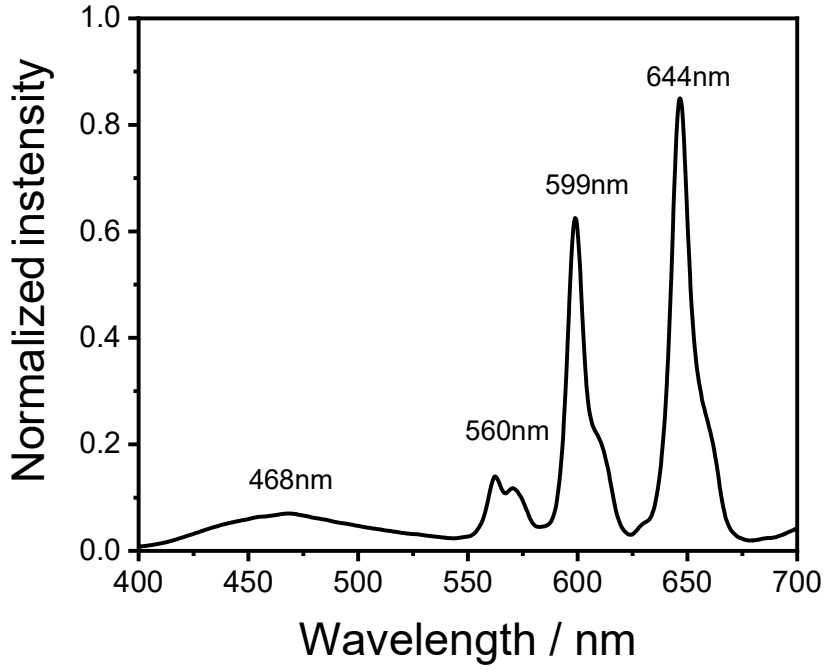

Figure S6. Solid-state photoluminescence spectrum of **ZnSm** at room temperature under 365 nm excitation.

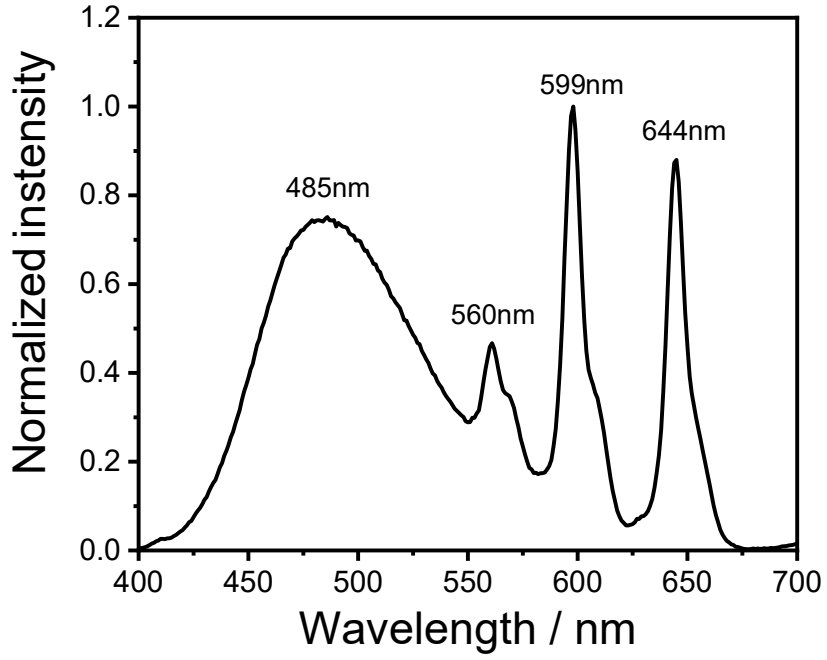

Figure S7. Emission spectrum of **ZnSm** in toluene at room temperature under 365 nm excitation.

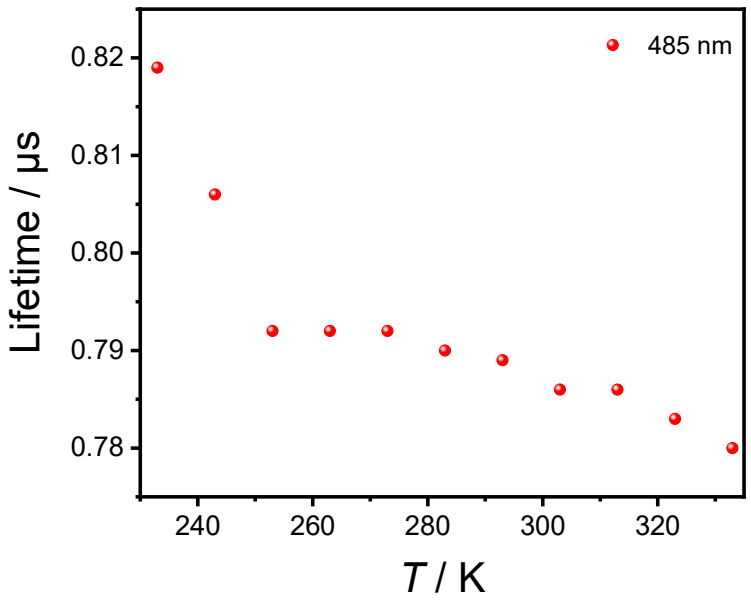

Figure S8. Temperature dependence of the luminescence lifetimes of the ZnL emission at 485 nm in **ZnSm**.

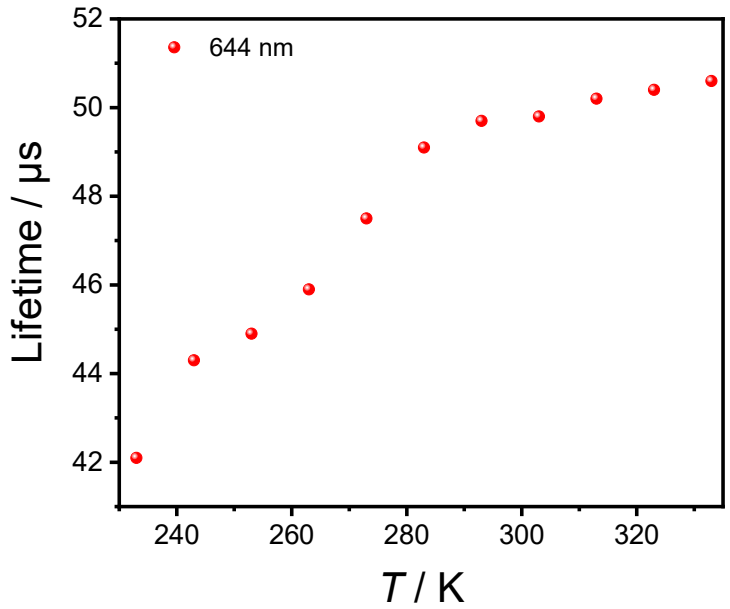

Figure S9. Temperature dependence of the luminescence lifetimes of the $^4G_{5/2} \rightarrow {}^6H_{9/2}$ transition of Sm^{3+} at 644 nm in **ZnSm**.

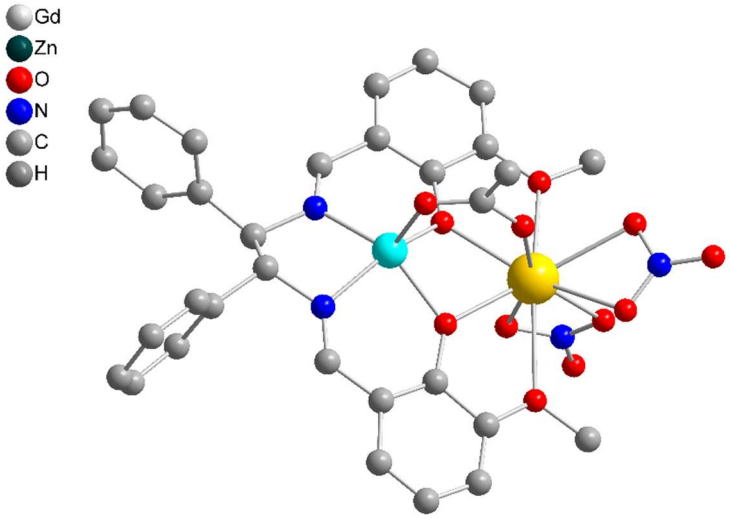

Figure S10. Molecular structure of **ZnGd**.

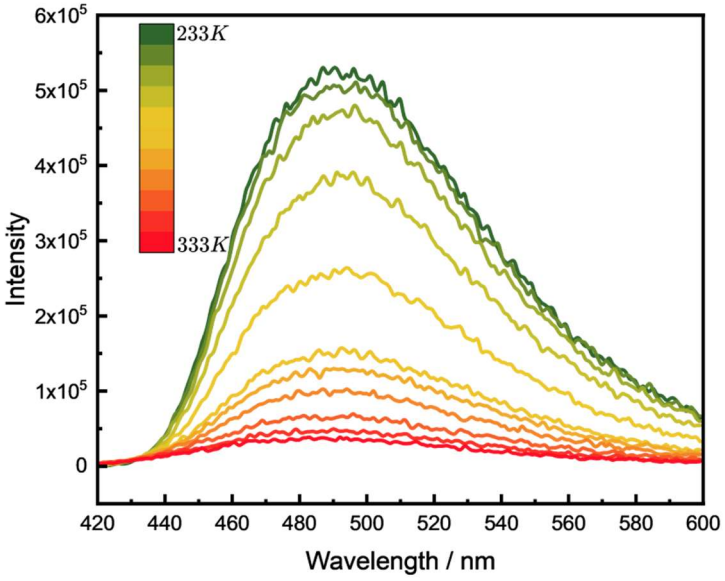

Figure S11. Temperature-dependent emission spectra of **ZnGd** in toluene (1.0×10^{-5} M) between 233 and 333 K under 365 nm excitation.

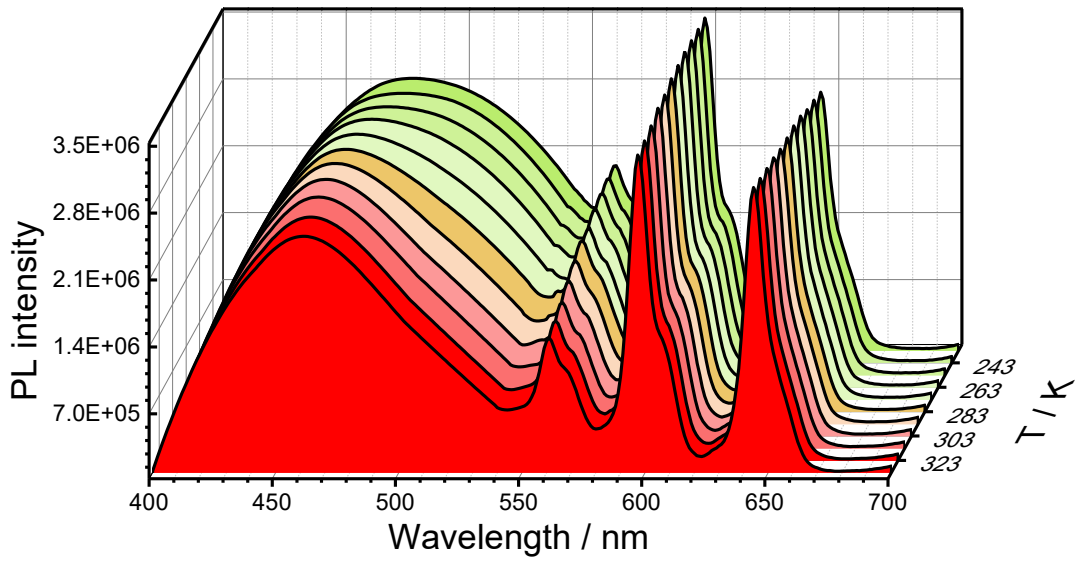

Figure S12. Temperature-dependent emission spectra of **ZnSm@PMMA** between 233 and 333 K under 365 nm excitation.

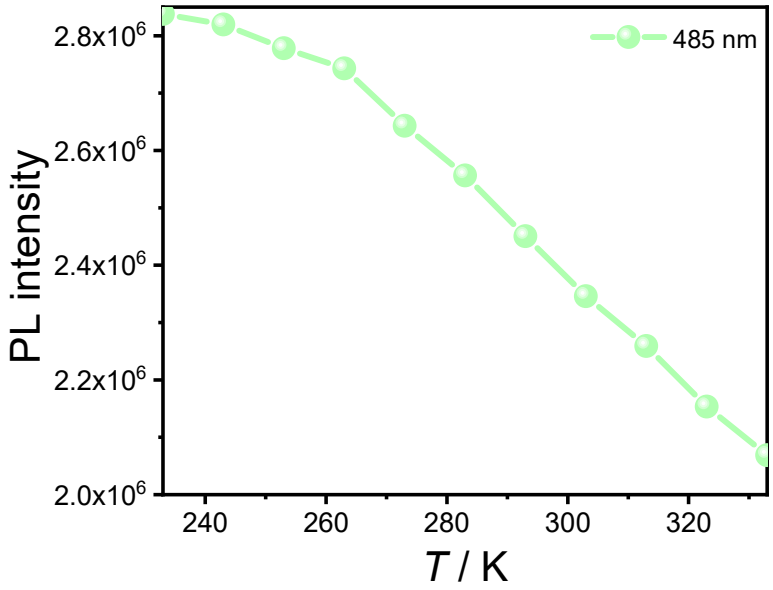

Figure S13.Temperature dependence of the photoluminescence (PL) intensity at 485 nm for **ZnSm@PMMA**. The solid line serves as a guide for the eye.

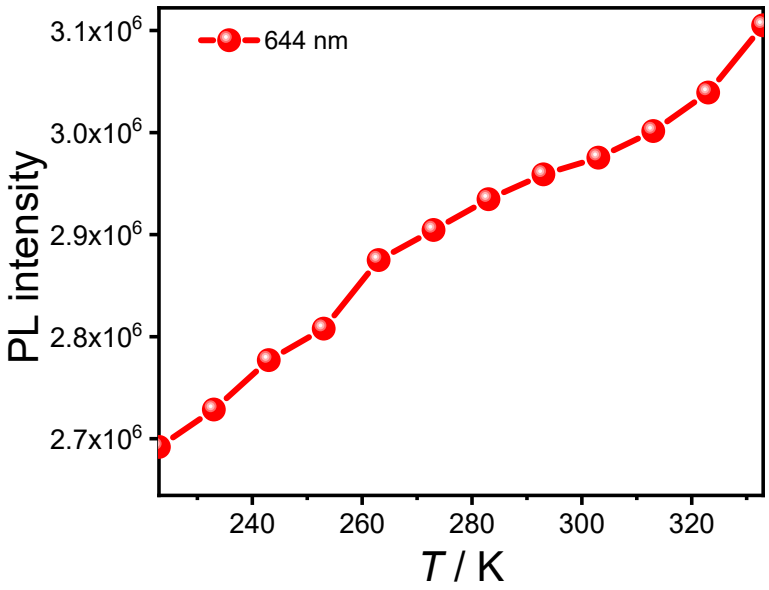

Figure S14. Temperature dependence of the PL intensity at 644 nm for **ZnSm@PMMA**. The solid line serves as a guide for the eye.

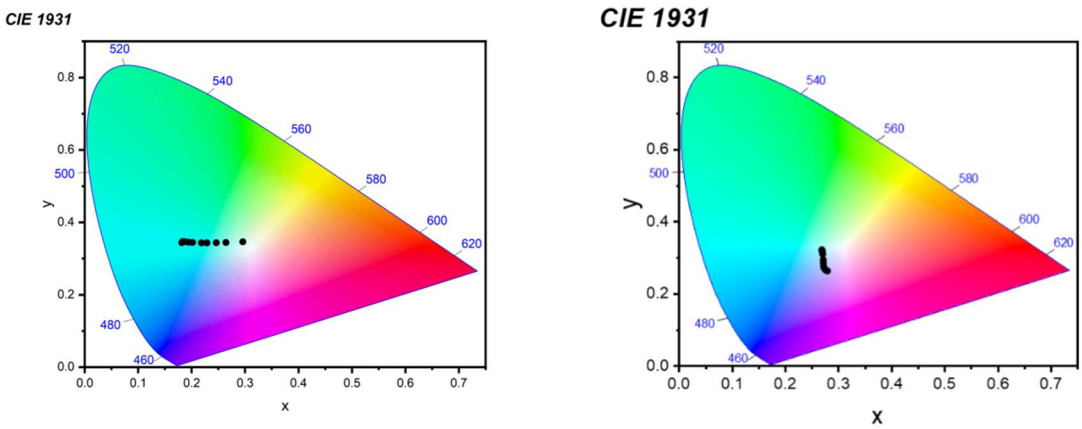

Figure S15. CIE chromaticity diagram showing the temperature-dependent luminescence color of **ZnSm** (left) and **ZnSm@PMMA** (right).

4. Supporting Tables

Table S1. Crystallographic data and refinement parameters for 1*R*,2*R*-ZnLSm(OAc)$(NO_3)_2$ (**ZnSm**), ZnLGd(OAc)$(NO_3)_2$ (**ZnGd**) and 1*R*,2*R*-ZnLGd(OAc)$(NO_3)_2$.

	1*R*,2*R*-ZnLSm(OAc)$(NO_3)_2$ (**ZnSm**)	ZnLGd(OAc)$(NO_3)_2$ (**ZnGd**)	1*R*,2*R*-ZnLGd(OAc)$(NO_3)_2$
Formula weight	877.31	884.21	884.21
Empirical formula	$C_{32}H_{29}SmN_4O_{12}Zn$	$C_{32}H_{29}GdN_4O_{12}Zn$	$C_{32}H_{29}GdN_4O_{12}Zn$
Temperature/K	150.0	180	293(2)
Crystal system	monoclinic	monoclinic	monoclinic
Space group	$P2_1$	$P2_1/n$	$P2_1$
a/Å	10.1405(3)	10.0973(3)	10.2413(8)
b/Å	19.2601(5)	19.1846(4)	19.4152(17)
c/Å	17.2094(6)	17.4270(4)	17.4296(12)
α/°	90	90	90
β/°	95.1850(10)	94.501(2)	94.748(6)
γ/°	90	90	90
Volume/Å^3	3347.36(18)	3365.42(14)	3453.8(5)
Z	4	4	4
ρ_{calc}g/cm^3	1.741	1.745	1.700
μ/mm^{-1}	2.523	2.735	2.665
F(000)	1748.0	1756.0	1756
Radiation	MoKα (λ = 0.71073)	MoKα (λ = 0.71073)	MoKα (λ = 0.71073)
2Θ range for data collection/°	4.034 to 52.79	2.2460 to30.2080	3.519 to 29.416
Index ranges	-12 ≤ h ≤ 12, -24 ≤ k ≤ 24, -21 ≤ l ≤ 21	-11 ≤ h ≤ 14, -24 ≤ k ≤ 26, -24 ≤ l ≤ 22	-13 ≤ h ≤ 13, -26 ≤ k ≤ 17, -22 ≤ l ≤ 15
Reflections collected	58670	37144	17282
Goodness-of-fit on F^2	1.077	1.107	0.990
Final R indexes [I>=2σ (I)]	R_1 = 0.0510, wR_2 = 0.1246	R_1 = 0.0348, wR_2 = 0.0683	R_1 = 0.0750, wR_2 = 0.0847
Final R indexes [all data]	R_1 = 0.0589, wR_2 = 0.1305	R_1 = 0.0465, wR_2 = 0.0716	R_1 = 0.1360, wR_2 = 0.1047
Largest diff. peak/hole / e Å^{-3}	2.551/-0.793	0.755/-0.723	1.333/-0.875
Flack parameter	0.017(9)		0.01(2)

Table S2. Selected bond distances (Å) for **ZnSm**.

	Sm–O	Zn–O	Zn–N
Sm1Zn1	2.493(10) 2.409(8) 2.630(9) 2.342(9) 2.642(8) 2.329(10) 2.517(10) 2.546(9) 2.465(10)	2.014(8) 1.971(9) 2.013(8)	2.044(10) 2.005(9)
Sm2Zn2	2.344(8) 2.331(10 2.629(9) 2.533(10) 2.469(9) 2.493(10) 2.632(10) 2.492(10) 2.355(9)	1.998(8) 1.972(9) 2.011(8)	2.025(9)

Table S3. Selected bond distances (Å) for **ZnGd**.

	Gd–O	Zn–O	Zn–N
ZnGd	2.350 (2) 2.610 (3) 2.314 (3) 2.616 (3) 2.319 (3) 2.501 (3) 2.484 (3) 2.453 (3) 2.463 (3)	2.004 (3) 2.019 (2) 1.980 (3)	2.024 (3) 2.014 (3)

Table S4. DFT calculated energy levels of ZnL moiety for **ZnSm**.

	E_{S1}–E_{S0} / cm^{-1}	E_{T1}–E_{S0} / cm^{-1}	E_{T1}–E_{S0} / nm
ZnY	28275	21101	473.9
ZnLa	28419	20595	485.6
ZnLu	28121	20829	480.1

Table S5. Calculated energy levels (cm^{-1}) of Sm^{3+} for **ZnSm** with inclusion of solvent effects.

$^6H_{5/2}$	$^6H_{7/2}$	$^6H_{9/2}$	$^6H_{11/2}$	$^6H_{13/2}$	$^6H_{15/2}$	$^6F_{1/2}$	$^6F_{3/2}$	$^6F_{5/2}$	$^6F_{7/2}$	$^6F_{9/2}$	$^6F1_{1/2}$	$^4G_{5/2}$	$^4G_{7/2}$
0	1117	2459	3874	5366	6779	7351	7389	7855	8725	9989	11429	18665	19668
160	1247	2511	3940	5449	6909		7445	7881	8765	10017	11481	19088	19847
324	1382	2656	4065	5519	7008			7915	8797	10067	11521	19607	20539
	1499	2720	4119	5606	7112				8833	10096	11549		20809
		2808	4173	5667	7150					10129	11568		
			4270	5708	7205						11602		
				5772	7252								
					7301								

Table S6. Calculated energy levels of Sm^{3+} (cm^{-1}) for **ZnSm** without inclusion of solvent effects.

$^6H_{5/2}$	$^6H_{7/2}$	$^6H_{9/2}$	$^6H_{11/2}$	$^6H_{13/2}$	$^6H_{15/2}$	$^6F_{1/2}$	$^6F_{3/2}$	$^6F_{5/2}$	$^6F_{7/2}$	$^6F_{9/2}$	$^6F1_{1/2}$	$^4G_{5/2}$	$^4G_{7/2}$
0	1134	2466	3874	5364	6767	7362	7404	7832	8711	9963	11446	18353	19291
176	1251	2515	3932	5431	6924		7455	7860	8750	9989	11492	18526	19363
326	1400	2675	4083	5533	7025			7903	8786	10038	11532	18720	20527
	1524	2736	4136	5626	7122				8815	10066	11561		20629
		2831	4184	5688	7154					10102	11588		
			4280	5720	7208						11624		
				5769	7240								
					7308								

Table S7. DFT calculated spin density of triplet excited (T_1) state of ZnL moiety for **ZnSm**.

	O5	C16	N23	C27	C31	C38	C45
ZnY	0.2526	0.4187	0.3228	0.2802	0.1773	0.1539	0.3577
ZnLa	0.2448	0.4342	0.3399	0.1529	0.2424	0.1813	0.3225
ZnLu	0.2558	0.4149	0.3226	0.2779	0.1754	0.1567	0.3535

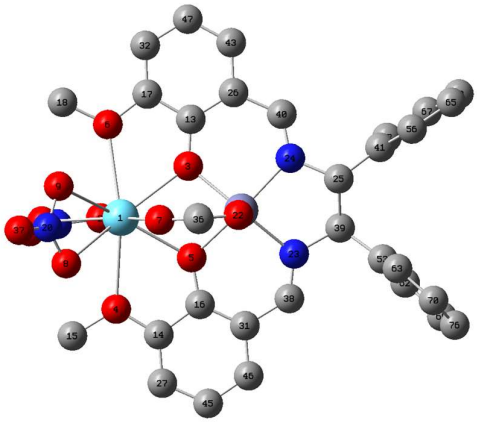

Table S8. Temperature sensing properties for selected ratiometric luminescent thermometers.

Thermometer[a]	Doped or not	Emission center	Maximum S_r (% K^{-1})	Temperature range (K, S_r>1%)	Ref
ZnSm	N	dual	3.4 (333 K)	253-333	**This Work**
Tb_2moshi_8': Sm_2moshi_8' = 1:1	Y	dual	3 (220 K)	150-350	*J. Am. Chem. Soc.* 2022, 144, 18259
$Tb_{0.1}Sm_{0.9}MC$	Y	dual	2.33 (278 K)	278-333	*Chem. Sci.* 2025, 16, 4821
Tb-MOFs@TGIC	MOF composite	dual	4.86 (~323 K)	273-323	*ACS Appl. Mater. Interfaces* 2023, 15,18114
$Na[(Gd_{0.8}Eu_{0.1}Tb_{0.1})SiO_4]$	Y	dual	2 (12 K)	~12-50	*J. Am. Chem. Soc.* 2015, 137, 3051
$[Dy_2(bpm)(tfaa)_6]$	N	dual	3.3 (~300 K)	~300-350	*ACS Cent. Sci.* 2019, 5, 1187
ZJU-88⊃perylene	Y	dual	1.28 (293 K)	293-353	*Adv. Mater.* 2015, 27, 1420
$Tb_{0.9}Eu_{0.1}PIA$	Y	dual	3.53 (300 K)	~250-300	*J. Am. Chem. Soc.* 2013, 135, 15559
$[Sm^{III}(H_2O)_3][Au^I(CN)_2]_3$	MOF	dual	1.08 (130 K)	——	*J. Mater. Chem. C* 2023, 11, 1008
		dual	1.78 (110 K)	~80-200	
TbMC	N	single	2.51 (333 K)	278-333	*Chem. Sci.* 2025, 16, 4821
$[NEt_4]_2[(Ph_4Si_4O_8)_2(Dy/Eu)_4(NO_3)_6(EtOH)_2(MeCN)_2]$ 4(MeCN)	Y	single	1.15 (293 K)	293-373	*RSC Adv.* 2023, 13, 26302
$[Yb_2(valdien)_2(NO_3)_2]$	N	single	1.1 (around 140 K)	80–320	*Chem. Sci.* 2019, 10, 6799
$[Yb(H_3L^{1,1,4})]\cdot 2MeOH$	N	single	0.15 (around 300 K)	——	*Inorg. Chem. Front.* 2020, 7, 3019
$\{[Ho^{III}_{0.11}Y^{III}_{0.89}(4\text{-pyridone})_4(H_2O)_2][Co^{III}(CN)_6]\}$	Y	single	6.9 (28 K)	25-140	*Chem. Sci.* 2021, 12, 730
$\{[Ho^{III}_{0.12}Y^{III}_{0.88}(4\text{-pyridone})_4(H_2O)_2][Rh^{III}(CN)_6]\}$	Y	single	2.7 (42 K)	25-130	*Chem. Sci.* 2021, 12, 730
$\{[Ho^{III}_{0.1}Y^{III}_{0.9}(4\text{-pyridone})_4(H_2O)_2][Ir^{III}(CN)_6]\}$	Y	single	4.6 (37 K)	35-144	*Chem. Sci.* 2021, 12, 730
$[YbCo(CN)_6(bpyO_2)_2(H_2O)_3]$	N	single	~0.1 (180 K)	——	*Dalton Trans.* 2022, 51, 8208
$Tb^{III}[Co^{III}(CN)_6]$	N	single	5.28 (15.9 K)	~20-92	*Angew. Chem. Int. Ed.* 2023, 62, e202306372
$[Tb^{III}(H_2O)_2][Co^{III}(CN)_6]\cdot 2.7H_2O$	N	single	5.49 (13.6 K)	~5-93	*Angew. Chem. Int. Ed.* 2023, 62, e202306372
$[Dy(acac)_3bpm]$	N	single	1.5 (70 K)	30-140	*Chem. Commun.* 2023, 59, 8723
$[Sm^{III}(H_2O)_3][Au^I(CN)_2]_3$	MOF	single	3.5 (80 K)	10-300	*J. Mater. Chem. C* 2023, 11, 1008
		single	2.67 (70 K)	~25-170	
$[DyCo(CN)_6(bpyO_2)_2(H_2O)_3]\cdot 4H_2O$	N	single	1.84 (70 K)	40-140	*Inorg. Chem.* 2022, 61, 2546
$(H_5O_2)_2(H)[Yb^{III}(hmpa)_4][Co^{III}(CN)_6]_2\cdot 0.2H_2O$	N	single	4.6 (50 K)	50-175	*J. Am. Chem. Soc.* 2020, 142, 3970
$[Dy_2(bpm)(tfaa)_6]$	N	single	14 (~300 K)	<12	*ACS Cent. Sci.* 2019, 5, 1187

[a] The names of the thermometers are quoted directly from the original literatures without modification.

5. References

1. Y. Jiang, L. Gong, X. Feng, W. Hu, W. Pan, Z. Li and A. Mi, *Tetrahedron*, 1997, **53**, 14327−14338.
2. *CrysAlisPro*, Version 1.171. 36.28; Agilent Technologies, Santa Clara, CA, 2013.
3. G. M. Sheldrick, *Acta Crystallogr. Sect. A: Found. Crystallogr.*, 2008, **64**, 112−122.
4. A. L. Spek, *J. Appl. Crystallogr.*, 2003, **36**, 7−13.
5. M. J. Frisch, G. W. Trucks, H. B. Schlegel, G. E. Scuseria, M. A. Robb, J. R. Cheeseman, G. Scalmani, V. Barone, G. A. Petersson, H. Nakatsuji, X. Li, M. Caricato, A. V. Marenich, J. Bloino, B. G. Janesko, R. Gomperts, B. Mennucci, H. P. Hratchian, J. V. Ortiz, A. F. Izmaylov, J. L. Sonnenberg, D. Williams-Young, F. Ding, F. Lipparini, F. Egidi, J. Goings, B. Peng, A. Petrone, T. Henderson, D. Ranasinghe, V. G. Zakrzewski, J. Gao, N. Rega, G. Zheng, W. Liang, M. Hada, M. Ehara, K. Toyota, R. Fukuda, J. Hasegawa, M. Ishida, T. Nakajima, Y. Honda, O. Kitao, H. Nakai, T. Vreven, K. Throssell, J. A. Montgomery, Jr., J. E. Peralta, F. Ogliaro, M. J. Bearpark, J. J. Heyd, E. N. Brothers, K. N. Kudin, V. N. Staroverov, T. A. Keith, R. Kobayashi, J. Normand, K. Raghavachari, A. P. Rendell, J. C. Burant, S. S. Iyengar, J. Tomasi, M. Cossi, J. M. Millam, M. Klene, C. Adamo, R. Cammi, J. W. Ochterski, R. L. Martin, K. Morokuma, O. Farkas, J. B. Foresman, D. J. Fox, Gaussian, Inc., Wallingford CT, 2016.
6. T. Yanai, D. Tew, N. Handy, Chem. Phys. Lett., 2004, **393**,51−57.
7. M. Dolg, H. Stoll, A. Savin, H. Preuss, Theor. Chem. Acc., 1989, **75**, 173−194.
8. M. Dolg, H. Stoll, H. Preuss, J. Chem. Phys., 1989, **90**, 1730−1734.
9. G. A. Petersson, M. A. Al-Laham, J. Chem. Phys., 1991, **94**, 6081−6090.
10. G. A. Petersson, A. Bennett, T. G. Tensfeldt, M. A. Al-Laham, W. A. Shirley, J. Mantzaris, J. Chem. Phys., 1988, **89**, 2193−2198.
11. F. Aquilante, J. Autschbach, R. K. Carlson, L. F. Chibotaru, M. G. Delcey, L. De Vico, I. Fdez Galván, N. Ferré, L. M. Frutos, L. Gagliardi, M. Garavelli, A. Giussani, C. E. Hoyer, G. Li Manni, H. Lischka, D.-X Ma, P.-Å. Malmqvist, T. Müller, A. Nenov, M. Olivucci, T. B. Pedersen, B.-D. Peng, F. Plasser, B. Pritchard, M. Reiher, I. Rivalta, I. Schapiro, J. Segarra-Martí, M. Stenrup, D. G. Truhlar, L. Ungur, A. Valentini, S. Vancoillie, V. Veryazov, V. P. Vysotskiy, O. Weingart, F. Zapata and R. Lindh, *J. Comput. Chem.*, 2016, **37**, 506–541.
12. B. O. Roos, R. Lindh, P.-Å. Malmqvist, V. Veryazov and P.-O. Widmark, *J. Phys. Chem. A*, 2004, **108**, 2851–2858.
13. B. O. Roos, R. Lindh, P.-Å. Malmqvist, V. Veryazov and P.-O. Widmark, *Chem. Phys. Lett.*, 2005, **409**, 295–299.
14. P. Å. Malmqvist, B. O. Roos and B. Schimmelpfennig, *Chem. Phys. Lett.*, 2002, **357**, 230–240.
15. B. A. Heß, C. M. Marian, U. Wahlgren and O. Gropen, *Chem. Phys. Lett.*, 1996, **251**, 365–371.
16. J. Finley, P. Malmqvist, B. O. Roos and L. Serrano-Andrés, *Chem. Phys. Lett.*, 1998, **288**, 299−306.